Catalysis Letters (2019) 149:3338–3348
https://doi.org/10.1007/s10562-019-02901-9

Enhanced Catalytic Performance of CuO–ZnO–Al_2O_3/SAPO-5 Bifunctional Catalysts for Direct Conversion of Syngas to Light Hydrocarbons and Insights into the Role of Zeolite Acidity

Tao Liu[1] · Tianliang Lu[2] · Mingming Yang[1] · Lipeng Zhou[1] · Xiaomei Yang[1] · Beibei Gao[1] · Yunlai Su[1]

Received: 4 May 2019 / Accepted: 10 July 2019 / Published online: 17 July 2019
© Springer Science+Business Media, LLC, part of Springer Nature 2019

Abstract

Synthesis of light hydrocarbons from synthesis gas using bifunctional catalysts consisting of CuO–ZnO–Al_2O_3 methanol synthesis catalysts and SAPO-5 were investigated in a fixed bed reactor. The operating results showed that both the temperature and the ratio of CZA/SAPO-5 influenced the CO conversion and the selectivity of the catalysts. The effects of different dehydration component such as HZSM-5, HMOR and SAPO-5 and subsequently the impact of the zeolite acidity on the catalytic performance were also investigated. Experimental results indicated that zeolites in bifunctional catalysts played the crucial role for the distribution of hydrocarbons, and SAPO-5 was superior to the other zeolites in terms of better conversion and C_3–C_5 selectivity due to its suitable topology and proper acidic property. The efficiency of the CZA/SAPO-5 catalysts was found to be directly proportional to the Brönsted acid sites density of the zeolite and Brönsted acid sites are the likely zeolite active sites for DME dehydration. High time–space yield (461.6 mg mL^{-1} h^{-1}) and high selectivity (88.1%) of light hydrocarbons (C_3–C_5) could be achieved on the CZA/SAPO-5-0.4 catalyst at 290 °C.

Graphic Abstract

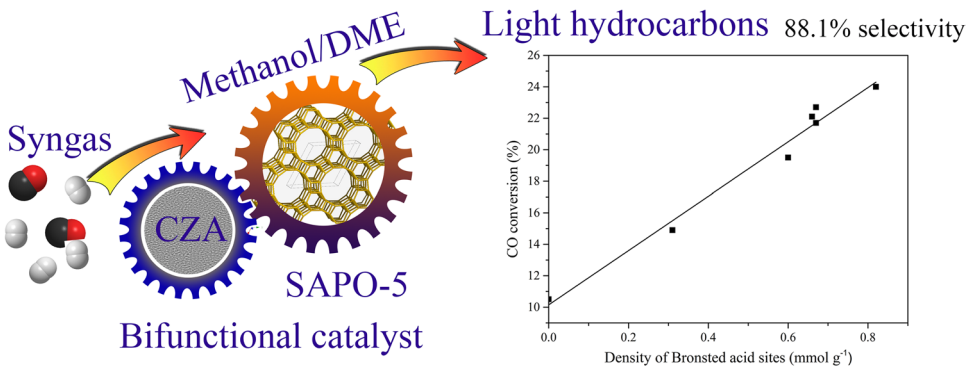

Keywords Synthesis gas · Light hydrocarbons · SAPO-5 · Acidity · Bifunctional catalyst

1 Introduction

Hydrocarbons [light olefins, liquefied petroleum gas (LPG), gasoline, etc.], sourced mainly from oil cracking, are very important energy resources and raw chemical feedstock for some industrially vital products and fine chemicals. With the depletion of petroleum and increasing demands for hydrocarbons, developing catalytic processes for the transformation

Electronic supplementary material The online version of this article (https://doi.org/10.1007/s10562-019-02901-9) contains supplementary material, which is available to authorized users.

✉ Beibei Gao
gaobeibei@zzu.edu.cn

✉ Yunlai Su
yunlaisu@zzu.edu.cn

Extended author information available on the last page of the article

of nonpetroleum carbon feedstocks such as natural gas, coal, and biomass into hydrocarbons for sustainable production of liquid fuels and chemicals becomes more attractive [1–3]. Syngas is a very versatile feedstock for the production of hydrocarbons, which can be derived from diverse carbon sources, such as natural gas, coal, biomass, and even municipal waste [4–7].

Fischer–Tropsch synthesis (FTS) is a conventional and typical process for the synthesis of hydrocarbons by hydrogenation of CO via syngas. Since its discovery in the 1920s, FTS process has received considerable attention. Fe, Co and Ru-based catalysts have been developed and related FTS mechanisms are investigated in depth [8–11]. The products of FTS are environmentally benign due to the characteristics of free of sulfur, nitrogen, and aromatics. However, due to the limitation of Anderson–Schulz–Flory (ASF) polymerization kinetics, FTS process usually gives a wide distribution of hydrocarbons with different chain lengths, which is particularly unselective towards the light hydrocarbons [12–15]. Thus, it is significant to develop alternative technologies to realize the selectivity control to produce narrowly distributed light hydrocarbons. Instead of the traditional FTS process, syngas can be transformed into light hydrocarbons through a multi-stage process (via methanol/dimethyl ether), which involves the transformation of syngas into methanol that is subsequently converted into hydrocarbons. This route could achieve a narrow distribution of hydrocarbons because the syngas-to-methanol (methanol synthesis) process and methanol-to-hydrocarbons (MTH) process are operated under their optimal conditions, respectively [16]. Furthermore, synthesis of hydrocarbons through intermediate methanol over a bifunctional catalyst containing both methanol synthesis active sites and dehydration active sites is a promising alternative route, in which syngas-to-methanol and MTH reactions could be coupled in a single process. Compared with the two-step process, the direct conversion of syngas into hydrocarbons would be more energy and cost efficient. Meanwhile, the formation of DME and the hydrocarbons would assist in overcoming the thermodynamic constraints inherent to methanol synthesis.

Generally, the extensively studied methanol synthesis catalysts include one or the combination of the following oxides CuO, Al_2O_3, ZnO and Cr_2O_3 [17–20]. Due to the high efficiency and industrialization, the more complex ternary CuO–ZnO–Al_2O_3 (CZA) catalysts have been commonly used for methanol synthesis [17, 21]. Compared to the methanol synthesis active component, dehydration active sites play a more critical role in the selectivity control of hydrocarbons. Consequently, studies of the direct synthesis of hydrocarbons from syngas have focused on investigating the influence of the acid components (typically a molecular sieve) on the distribution of products and there are many examples in previous reports of the use of the bifunctional catalyst to obtain different products. In general, SAPO-34 are used as the molecular sieve component within the bifunctional catalyst to achieve C_2–C_4 hydrocarbons [16, 22, 23], while C_3–C_4 hydrocarbons are typically favored using Beta [24–26] or Y zeolites [27–29]. Besides, gasoline-range hydrocarbons can be made using HZSM-5 [30–33] or H-ferrierite [34]. In short, the pore size and topology of the methanol conversion component may influence the distribution of products and hence the hydrocarbons selectivity could be regulated by choosing the appropriate molecular sieve component. Additionally, the acidic strength and acid density of zeolites are also expected to have significant effects on the formation of active intermediates and side reactions in the methanol conversion, and thus affect the hydrocarbons selectivity [35]. Wang et al. made a comparative study of PdZSM-5, Pdβ, and PdY in hybrid catalysts to convert syngas to hydrocarbon. They found that the dehydration step of DME in the syngas to hydrocarbon mainly occurred on the Brönsted acid sites of the Pd zeolite [36]. Cheng et al. reported that the decrease in the density of Brönsted acid sites could suppress the hydrocracking and isomerization reactions in the syngas into gasoline-range hydrocarbons reaction [3]. It was clarified that both the acidity and mesoporosity played critical roles in controlling the hydrocracking reactions and contributed to the improved product selectivity in FT synthesis. Moreover, they proposed that the strong acid site was responsible for the aromatization reaction and a larger density of strong acid sites reduced the selectivity of aromatics and increased that of C_2–C_4 paraffins in the one-step conversion of syngas into aromatics [37]. Thus appropriate pore structure and the proper acidity are crucial for the selectivity of light hydrocarbons.

SAPO-5, a 12-membered-ring molecular sieve with a relatively large pore size (0.73 nm × 0.73 nm), allow the formation of products (C_3–C_{5+}) with larger molecular size, while its moderate strength can suppress the formation of methane and the occurrence of side reactions which form heavy products and aromatic coke molecules. In this work, a series of bifunctional catalysts CZA/SAPO-5 were prepared by a physical mixture method and their enhanced catalytic performance were verified. First, a comparative study of syngas conversion over bifunctional catalysts containing SAPO-5 and other different types of zeolites were carried out to explain the reason for the superiority of SAPO-5 zeolite over the other zeolites. Then, we investigated the effect of operating temperature and the ratio of CZA/SAPO-5 in bifunctional catalysts on the catalytic activity. The catalytic performance of SAPO-5 zeolites of which the zeolite acidities were systematically varied was also investigated to assess the influence of the acid property of SAPO-5 on the activity and selectivity during the syngas to hydrocarbon process.

2 Experimental

2.1 Materials

HZSM-5 (nSi/nAl = 28.3), HMOR (nSi/nAl = 13.0) and HY (nSi/nAl = 2.6) zeolites were purchased from Nankai University Catalyst Co., Ltd. $Cu(NO_3)_2{\cdot}3H_2O$, $Zn(NO_3)_2{\cdot}6H_2O$, $Al(NO_3)_3{\cdot}9H_2O$, triethylamine (TEA, 99%) and tetraethyl orthosilicate (TEOS) were of analytic grade and obtained from Sinopharm Chemical Reagent Co., Ltd. Pseudoboehmite (78.4 wt% Al_2O_3), H_3PO_4 (85 wt%) and Na_2CO_3 were of analytic grade and used as received.

2.2 Catalyst Preparation

Methanol synthesis catalyst of CuO–ZnO–Al_2O_3 (mass ratio of Cu:Zn:Al = 40:33:27) were prepared by co-precipitation method. Aqueous $Cu(NO_3)_2$ (1.0 mol L^{-1}), $Zn(NO_3)_2$ (1.0 mol L^{-1}) and $Al(NO_3)_3$ (1.0 mol L^{-1}) solution and the aqueous of precipitator (Na_2CO_3, 1.0 mol L^{-1}) were added drop-wise into a beaker containing water simultaneously at 60 °C. After aging at 60 °C for 5 h, the obtained precipitate was filtered and washed thoroughly with deionized water. Finally, the prepared samples were dried at 120 °C for 12 h and calcined at 320 °C for 5 h. After pressing, crushing and sieving, particles with 20–40 mesh were obtained. The prepared CuO–ZnO–Al_2O_3 catalysts were denoted as CZA.

SAPO-5 samples were prepared by hydrothermal method with the following gel composition: 1.55 TEA: 1.0 Al_2O_3: 1.0 P_2O_5: x SiO_2: 50 H_2O, where x = 0.1, 0.2, 0.3, 0.4, 0.5 and 0.6, respectively. Typically, calculated amount of pseudoboehmite was added to deionized water under stirring, followed by the addition of tetraethyl orthosilicate. After stirring for 1 h, phosphoric acid was added and stirred for 20 h. After further addition of TEA dropwise, the mixture was stirred for 2–4 h and the obtained gel was crystallized at 170 °C for 40 h in a stainless-steel autoclave lined with polytetrafluorethylene. After the crystallization, the SAPO-5 products were filtered, washed with deionized water, dried at 100 °C for 12 h, and calcined at 550 °C in air for 24 h. The obtained samples were denoted as SAPO-5-x, where x represents the molar ratio of SiO_2/Al_2O_3 in the initial gels.

CZA/SAPO-5, CZA/HMOR, CZA/HY and CZA/HZSM-5 were prepared by physically mixing the CZA methanol synthesis catalyst with SAPO-5, HMOR, HY and HZSM-5 respectively. After grinding, the samples were pressed and crushed. Particles with 20–40 meshes were collected for the experiments.

2.3 Catalyst Characterization

X-ray diffraction (XRD) patterns of the samples were collected on a Panalytical X'Pert PRO instrument with Cu Kα (λ = 0.154059 nm) radiation operated at 40 kV and 40 mA. Chemical compositions of the solid samples were determined with a Philips Magix-601 X-ray fluorescence (XRF) spectrometer. N_2 adsorption–desorption measurements of the catalysts were carried out on a Quantachrome Autosorb at − 196 °C. Before measurements, the samples were degassed at 150 °C for 1.5 h. The total surface area was calculated based on the BET equation. The micropore volume, external surface area and micropore surface area were evaluated by using the t-plot method. Temperature-programmed desorption of ammonia (NH_3-TPD) was performed on a Micromeritics AutoChem II 2920 instrument with a heating rate of 10 °C min^{-1} at a temperature ramp from 120 to 600 °C. The sample weight was about 100 mg. The FTIR spectra of the samples with pyridine adsorption were collected with a Bruker Tensor II spectrometer with the resolution of 4 cm^{-1}. Typically, the samples (13–14 mg) were pretreated at 450 °C for 3 h after evacuation to remove water. After the pool was cooled to room temperature, the FTIR spectrum of the sample was recorded as a background reference. Then, pyridine gas was charged into the pool until adsorption saturation (15 min). Subsequently, pyridine was desorbed from the sample by evacuation at different temperatures. After that, the spectrum of the sample with pyridine adsorption (pyridine-FTIR) was collected using the obtained spectrum as the reference.

2.4 Catalytic Tests

Catalytic conversion of syngas to light hydrocarbons was carried out on a fixed-bed stainless-steel micro-reactor with 6 mm inner diameter. Activation of the catalyst was carried out under reactant syngas containing 64.1 vol% H_2, 26.7 vol% CO and 6.3 vol% CO_2, with a small amount of CH_4, O_2 and H_2O (O_2 and H_2O were removed before use). Typically, after addition of the catalysts into the reactor, the reactant gas was charged. Then, the reactor was heated from room temperature to 320 °C in 3 h and then keeping at 320 °C for 2 h. After the reactor was cooled to reaction temperature, the syngas was input under the desired reaction pressure and GHSV. Products were analyzed on an on-line gas chromatograph (GC) with a 4 mm × 2 m stainless-steel GDX-103 (40–60 mesh) packed column and an FID detector.

3 Results and Discussion

3.1 Characterization

3.1.1 Textural and Structural Properties of the Zeolites

XRD patterns of the synthesized SAPO-5 samples are shown in Fig. S1. All the samples display the reflections characteristic for AFI crystalline structures, confirming the highly crystalline nature of the samples and the purity of the samples. The chemical compositions as well as the textural properties of the zeolites are summarized in Table 1 and Table S1. It can be seen that the bulk Si/Al ratios of SAPO-5-x samples determined with XRF increase with molar ratio of Si/Al in the initial gels. The textural parameters of SAPO-5-x and the related aluminosilicate zeolites determined by N_2 adsorption–desorption measurements are also listed in Table 1. It indicates that SAPO-5 samples with different Si content have similar surface area and total pore volume, while the surface area of the aluminosilicate zeolites varied with their topological type. The BET area of HY is 632 $m^2\ g^{-1}$, much larger than that of HZSM-5 (274 $m^2\ g^{-1}$). Besides, the micropore volume of HZSM-5 (0.14 $cm^3\ g^{-1}$) is close to that of HMOR (0.18 $cm^3\ g^{-1}$), smaller than that of HY. In a word, the macrospore volume and macrospore area of zeolites with different topological type varied in the following order: HY > HMOR > HZSM-5 > SAPO-5. The free diameters of the zeolite channels are also given in Table 1.

3.1.2 Acid Properties of the Zeolites

Since acid property of the catalyst has great effect on its activity, selectivity and resistance to deactivation in methanol/DME dehydration [38], the acidities of the zeolites are of much interest and should be comprehensively investigated. NH_3-TPD technique was used to characterize the acidity and strength of acid sites of the catalysts and the corresponding profiles are shown in Fig. 1 and Fig. S2.

The desorption temperatures signify the strength of acid sites, while the area under the curves indicates the amount of ammonia desorbed. It can be seen that all the samples present two desorption peaks, which are in accordance with the data already reported in the literature [39]. The former peak corresponds to the desorption of physisorbed NH_3 and NH_3 adsorbed on lattice defects or terminal hydroxyl groups, whereas the high temperature peak should mainly arise from the NH_3 desorption from the strong acid sites. Obviously, NH_3 is retained up to 550 °C in the case of HZSM-5 and even up to 700 °C in the case of HMOR. Therefore, based on the TPD results, we could rank the acid strength of the zeolites in the following decreasing order: HMOR > HZSM-5 > HY > SAPO-5. However, NH_3 adsorbed on AlPO-5 desorbes below 200 °C, indicating the absence of strong acid sites. After deconvolution of the TPD plots with Gaussian curves, amount of acid sites with different strength was calculated according to the corresponding peak area and the results are listed in Table 2 and Table S2. According to these values, the concentration of medium/strong acid sites gradually increases for the sample with Si/Al ratio less than 0.14, in agreement with the increasing Si content. However, with further increasing Si content, the total medium/strong acid amount decreases slightly, while centers of desorption peaks corresponded to medium and strong acid sites shift to higher temperature. It can be explained by the fact that Si can be incorporated into framework through substitution for one phosphorous in the aluminophosphate framework (SM2 mechanism) when the Si/Al ratio is relatively low, which leads to the formation of the Brönsted acidity of SAPO-5 [39]. When increasing the Si content, both SM2 and SM3 substitution mechanisms occur and give rise to aluminosilicate domains (commonly

Table 1 Textural and structural properties of the samples

Sample	Size of channels (Å × Å)	n(Si)/n(Al)[a]	S^b_{BET} ($m^2\ g^{-1}$)	S^c_{micro} ($m^2\ g^{-1}$)	V^d_{total} ($cm^3\ g^{-1}$)	V^c_{micro} ($cm^3\ g^{-1}$)
SAPO-5-0.1	7.3 × 7.3	0.032	251	138	0.25	0.072
SAPO-5-0.3	7.3 × 7.3	0.09	300	194	0.23	0.10
SAPO-5-0.4	7.3 × 7.3	0.14	272	218	0.18	0.11
SAPO-5-0.6	7.3 × 7.3	0.25	294	162	0.27	0.084
HZSM-5	5.1 × 5.5 [100] 5.3 × 5.6 [010]	28.3	274	274	0.14	0.14
HMOR	6.5 × 7.0	13	448	343	0.32	0.18
HY	7.4 × 7.4	2.6	632	540	0.40	0.30

[a]Determined by X-ray fluorescence (XRF) analysis

[b]BET surface area

[c]S_{micro} (micropore area) and V_{micro} (micropore volume) determined by the t-plot method

[d]V_{meso} (mesopore volume) = $V_{total} - V_{micro}$, V_{total} is determined from adsorbed volume at $P/P_0 = 0.98$

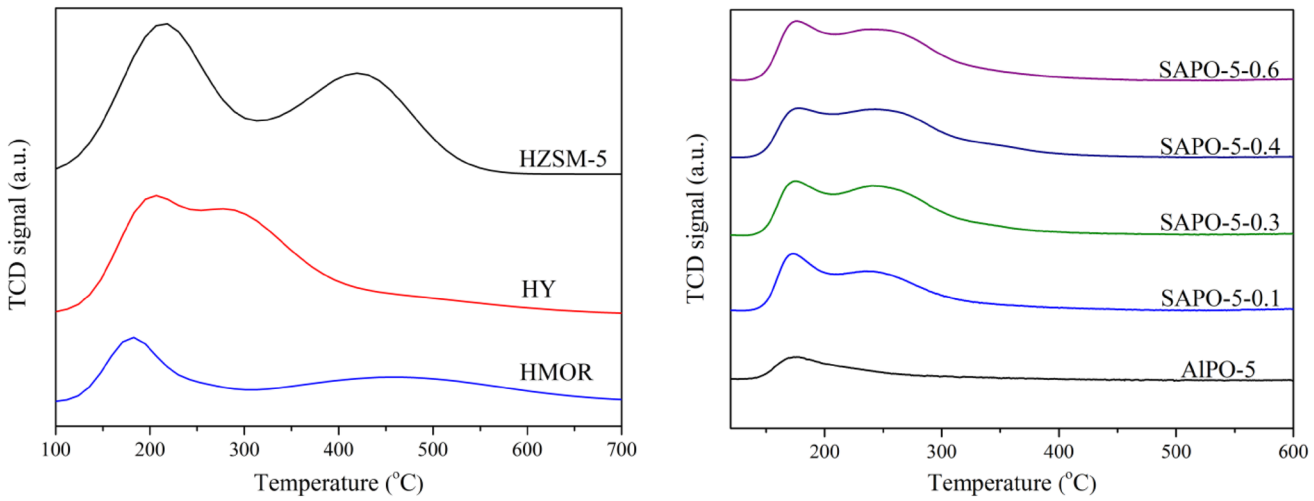

Fig. 1 NH_3-TPD profiles of HZSM-5, HY, HMOR (**a**) and SAPO-5-*x* (**b**)

Table 2 Acid properties of the SAPO-5-*x* samples with different Si/Al ratio

Sample	Total acid sites (mmol g^{-1})[a]	Weak acid sites (mmol g^{-1})[a]	Medium and strong acid sites (mmol g^{-1})[a]	C_B (mmol g^{-1})[b]	C_L (mmol g^{-1})[b]
AlPO-5	0.19	0.19	0	0	0.19
SAPO-5-0.1	0.60	0.32	0.28	0.31	0.29
SAPO-5-0.3	1.01	0.46	0.55	0.67	0.34
SAPO-5-0.4	1.12	0.46	0.66	0.82	0.30
SAPO-5-0.6	0.99	0.44	0.55	0.66	0.33

[a]Density of the acid sites, determined by NH_3-TPD. Weak acid sites, medium acid sites and strong acid sites were differentiated according to the desorption temperatures

[b]The density of L and B acidity was calculated from both the molar ratio of the amount of Lewis acid sites to that of Brönsted acid sites (L/B) and total acid sites determined by NH_3-TPD. The L/B value was calculated according to the area of the corresponding peak measured at a pyridine desorption temperature of 200 °C

referred to Si islands) in the SAPO network, leading to less acid centers but higher strength than the one arising only from the SM2 substitution. Moreover, as listed in Table S2, aluminosilicate zeolites (HY, HMOR and HZSM-5) have more acid sites than SAPO-5. To be specific, there are the most acid sites in HY (3.56 mmol g^{-1}) due to the low Si/Al mole ratio, while the number of total acid sites on HMOR (1.87 mmol g^{-1}) is the minimum in aluminosilicate zeolites.

In consideration of the different roles of Brönsted and Lewis acid sites in conversion of syngas to hydrocarbons, pyridine-FTIR was further applied to differentiate B and L acid sites in the zeolites (Fig. 2 and Fig. S2). It can been seen that IR bands at 1450 (or 1453) cm^{-1}, 1546 (or 1545) cm^{-1} and 1490 cm^{-1} are observed in the spectra, which are ascribed to pyridine adsorption on the Lewis (L) acid sites, Brönsted (B) acid sites and both L and B acid sites, respectively. The molar ratio of L acid sites to B acid sites (L/B) is calculated according to the integrated areas of the corresponding peaks in the IR spectra following the procedures reported in the literature [40]. In view of that total acid sites density determined by IR is less accurate, the densities of L and B acid sites of SAPO-5 samples were calculated according to the L/B ratio identified by pyridine-FTIR and total acid sites density determined by NH_3-TPD. The results are listed in Table 2 and Table S2. For SAPO-5-x, the Lewis acid density shows little change when the Si/Al ratio varies, while increase of Si content in the SAPO-5 leads to a significant increase of the Brönsted acid density when the Si/Al ratio is less than 0.14. However, further increasing the Si content give rise to the decrease of the Brönsted acid density, in accord with the variation trend of the total medium/strong acid amount, which can be illustrated by the mechanism of Si substitution in SAPO molecular sieves as well. As expected, there is no Brönsted acid site in AlPO-5 because of the absence of Si in the framework. Aluminosilicate zeolites (HY, HMOR and HZSM-5) have more Brönsted and Lewis acid sites than SAPO-5 (Table S2). Specifically, the

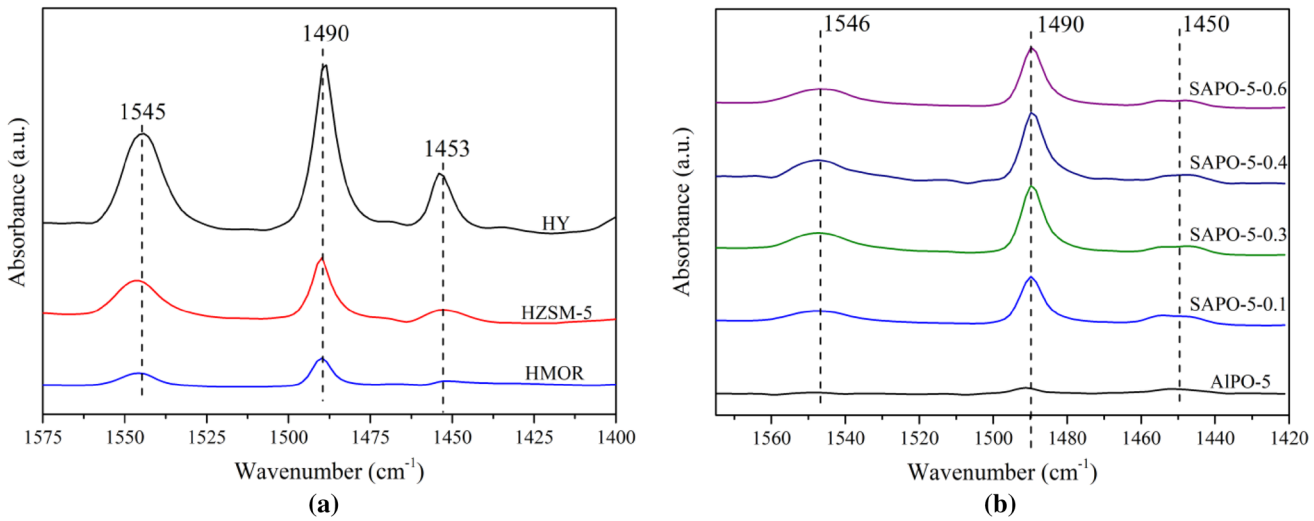

Fig. 2 IR spectra of of HY, HZSM-5, HMOR (**a**) and SAPO-5-x (**b**) after pyridine adsorption

Brönsted acid density of HY (2.64 mmol g^{-1}) is greatest due to the low Si/Al mole ratio, while that of HMOR (1.42 mmol g^{-1}) is the minimum in aluminosilicate zeolites.

3.2 Catalytic Performance of the One-Step Syngas Conversion

3.2.1 Catalytic Performance of the CZA/Zeolite Bifunctional Catalysts: Effect of the Zeolite Structure

Generally, the syngas to hydrocarbon process over a bifunctional catalyst of CZA/zeolite mainly involves the following reactions [28]: (1) CO hydrogenation to methanol, (2) methanol dehydration to DME, (3) DME further dehydration to final hydrocarbon products, and (4) water–gas shift (WGS) reaction. The relevant reactions are as follows:

$$CO + 2H_2 \leftrightarrow CH_3OH \quad (1)$$

$$2CH_3OH \leftrightarrow CH_3OCH_3 + H_2O \quad (2)$$

$$nCH_3OCH_3 \leftrightarrow C_nH_{2n+2} + nH_2O \quad (3)$$

$$CO + H_2O \leftrightarrow CO_2 + H_2 \quad (4)$$

Overall reaction:

$$2nCO + (n+1)H_2 \leftrightarrow C_nH_{2n+2} + nCO_2 \quad (n = 1, 2, \ldots, 6). \quad (5)$$

Reactions (1) and (4) are catalyzed by a methanol synthesis catalyst, and Reactions (2) and (3) are catalyzed by an acid catalyst. Methanol synthesis from syngas is restricted by thermodynamic equilibrium [41]. CO conversion could be increased in the syngas to hydrocarbon process due to in situ methanol removal to form DME and the hydrocarbons, where the thermodynamic constraint inherent to methanol synthesis is broken. Therefore, the direct synthesis of the hydrocarbons could be performed over a bifunctional catalyst composed of two components. Given that the product distributions depend significantly on the topology of the zeolites used in the bifunctional catalysts, the effects of using different zeolites were investigated and comparative results when mixing CZA with HZSM-5, HY, HMOR and SAPO-5 are shown in Table 3. Clearly, the activity and selectivity of the catalysts are remarkably affected by the zeolite employed. From the detailed information about the pore size of the four zeolites given in Table 1, it can be seen that the pore size order of the four zeolites is as follows:

Table 3 Hydrocarbon distribution over CZA/HZSM-5, CZA/HY, CZA/HMOR and CZA/SAPO-5

Catalyst[a]	X_{CO} (%)	Hydrocarbon product distribution (%)						Iso-C_4/C_4 (%)
		C_1	C_2	C_3	C_4	C_5	C_{6+}	
CZA/HZSM-5	12.0	25.7	36.4	9.1	20.2	8.6	0	2.32
CZA/HY	17.9	6.5	11.6	22.2	40.2	13.2	6.3	0.70
CZA/HMOR	14.5	5.6	22.3	44.5	19.1	5.2	3.3	1.58
CZA/SAPO-5-0.4	24.4	3.2	5.4	28.0	48.1	12.0	3.3	2.80

Reaction conditions: $p = 4.0$ MPa, $GHSV = 9600\ h^{-1}$, $n(H_2)/n(CO) = 2.3$, $T = 290$ °C, reaction time 1 h

[a]Mass ratio of CZA: zeolite = 1:4

HY > SAPO-5 > HMOR > HZSM-5. Correspondingly, more C_{5+} hydrocarbons were produced over the CZA/HY and CZA/SAPO-5 catalyst, consistent with their larger pore size. In contrast, CZA/HZSM-5 showed the highest selectivity for ethane and CZA/HMOR gave the highest selectivity for propane, which can be attributed to the stronger Brönsted acid sites that would promote the cracking of higher hydrocarbons to smaller fractions which occur over zeolites [36]. Remarkably, SAPO-5 gave a much larger fraction of C_3–C_5 alkanes (88.1%) than the other three aluminosilicate zeolites and over 74% of the C_4 fractions were isobutane.

The yield of the CO hydrogenation products over different catalysts is given in Table S3. A large amount of DME was observed in the CZA/HY and CZA/HZSM-5 catalytic systems. Provided that the methanol dehydration to DME and the DME dehydration to hydrocarbons take place on the weak Lewis acid sites and Brönsted acid sites respectively, the existence of the intermediate products DME in the final products may be associated with the L/B ratio of the zeolites. As shown in Table S2, the L/B ratios are the same for HY (0.35) and HZSM-5 (0.35). According to the above results, we propose that the intermediate products DME could not further dehydrated to hydrocarbons in time on the Brönsted acid sites of HY and HZSM-5. It is expected since that the reaction of methanol dehydration to DME could occur at lower temperature and the conversion is between 90 and 100% during the temperature range of 150–400 °C, while the Brönsted acid sites in HY and HZSM-5 for DME dehydration tend to be less active at temperature equal to 290 °C. Thus, lower L/B ratio or higher temperature is required to ensure total conversion of DME for aluminosilicate zeolites under these conditions. According to the previous report that at the typical syngas-to-DME reaction temperature (260 °C), the strong Brönsted acid sites are the likely zeolite active sites for methanol dehydration to DME [42], we speculate that Brönsted acid sites are also responsible for DME formation in methanol dehydratione. Notably, when CZA/SAPO-5-0.4 was used as the catalyst, both high products yield (461.6 mg mL^{-1} h^{-1}) and high selectivity (88.1%) of C_3–C_5 were obtained, in spite of its relatively low acid site density and mild acidity. Yuen et al. compared aluminosilicate and silicoaluminophosphate versions of AFI and CHA structured catalysts and concluded that the pore-size was a more important factor than acid strength in MTH reaction [43]. Olsbye et al. also found that the moderately acidic H-SAPO-5 catalyst differed from large-pore zeolites studied previously as the absence of cavities and intersections which facilitates formation of the space available for reactions [44]. They proposed that the MTH reaction proceeded through a dual cycle mechanism on SAPO-5, where the arene cycle was assumed to account for production of the lightest alkenes while the alkene cycle produced the heavier alkenes [44]. The alkene cycle was more important in H-SAPO-5 than in large-pore catalysts of higher acid strength, which accounts for the formation of C_3–C_5 alkenes and isobutene in the products of reaction. On the other hand, Olsbye et al. revealed the moderately acidic H-SAPO-5 was more selective towards C_3–C_5 hydrocarbons as compared to the strongly acidic H-SSZ-24 that produced more C_2–C_3 hydrocarbons [45]. Therefore, the high activity of the bifunctional catalyst with SAPO-5 zeolite could be attributed to its appropriate topological structure and moderate acidity, which are essential for formation of hydrocarbons. It indicates that zeolite in bifunctional catalyst plays the critical role for distribution of product hydrocarbons, and SAPO-5 is more suitable for synthesis of light hydrocarbon from synthesis gas.

3.2.2 Catalytic Performance of the CZA/SAPO-5 Bifunctional Catalysts: Effect of the Temperature

Reaction temperature plays a vital role for the catalytic performance of catalyst. Thus, syngas conversion was measured over physically mixed CZA and SAPO-5-0.4 as a function of temperature when operating at 4 Mpa. As shown in Table S4 and Fig. 3, the CO conversion increased from 9.9 to 24.4% when the temperature increased from 260 to 290 °C. At 260 °C, the product analysis showed that the intermediate DME (11.8% selectivity) existed in the product, indicating the low dehydration ability of SAPO-5. It is reasonable since the methanol-to-hydrocarbon process is typically conducted at a higher temperature to ensure total conversion of methanol/DME. When the temperature was elevated to 270 °C, complete conversion of DME could be achieved. Further increasing the temperature to 290 °C, the CO conversion continued to rise. However, when the temperature increased from 300 to 320 °C, the CO conversion

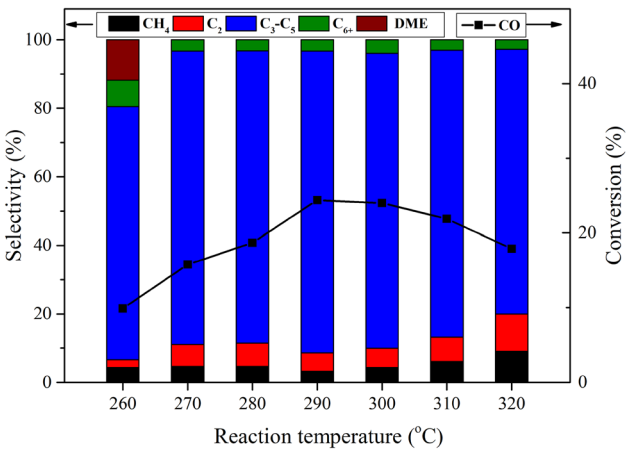

Fig. 3 Effect of reaction temperature on CO conversion and product selectivity for conversion of syngas to light hydrocarbons on CZA/SAPO-5-0.4. Reaction conditions: mass ratio of CZA: SAPO-5 = 1:4; p = 4.0 MPa, $GHSV$ = 9600 h^{-1}, $n(H_2)/n(CO)$ = 2.3, reaction time 1 h. *DME* dimethyl ether

decreased. Considering that CZA catalysts tend to deactivate at temperatures greater than 300 °C due to sintering of the Cu particles, and the CO conversion for this hybrid catalyst is rather low at 320 °C, we speculated that the conversion decrease at 320 °C is more likely due to catalyst deactivation. To further confirm the conclusion, additional experiments were carried out. It revealed that when decreasing the temperature to 290 °C after operated at 320 °C, the CO conversion for the composite catalyst didn't recover, indicating its deactivation. Also, as shown below in Fig. S3, the CuO/ZnO/Al_2O_3–SAPO-5 catalyst system was significantly unstable under the high Gas hourly space velocity (GHSV) of 9800 h^{-1}. The catalyst system was relatively stable over the course of 11 h or more when decreasing the GHSV to 7000 h^{-1}. It is not surprising in consideration of the instability of the CuO/ZnO/Al_2O_3 catalyst under syngas at relatively high temperatures [46]. The more sintering-resistant Pd/ZnO/Al_2O_3 catalyst will be used in our future study.

Temperature is also of primary importance in hydrocarbon distribution (Fig. 3). It shows that hydrocarbon yield and C_3–C_5 selectivity increased as reaction temperature increased from 260 to 290 °C, and then decreases as reaction temperature increased from 290 to 320 °C. Furthermore, when the reaction temperature increases from 290 to 320 °C, C_3–C_5 hydrocarbons selectivity decreased with increasing temperature while methane (C_1) selectivity increased due to increased CO methanation activity with temperature. Meanwhile, high temperature accelerated the cracking of C_{6+} hydrocarbons, leading to the decrease of heavy hydrocarbons and the increase of C_2 hydrocarbons. Furthermore, selectivity of iso-C_4H_{10} and iso-C_5H_{12} decreased in C_3 to C_5 hydrocarbons, while C_3H_8 increased with the reaction temperature (Table S5). The effects of reaction temperature on catalytic performance of physically mixed CZA and SAPO-5 with different Si/Al ration were also investigated and shown in Fig. S4. These results highlighted the importance of operating at lower temperature and 300 °C was applied as the optimized reaction temperature in the following study.

3.2.3 Catalytic Performance of the CZA/SAPO-5 Bifunctional Catalysts: Effect of the Mass Ratio of SAPO-5 to CAZ in the Bifunctional Catalysts

The results reported above were all achieved with a CZA: SAPO-5 ratio of 1:4 by weight. In the experiments, there was negligible DME in the products, suggesting that the amount of SAPO-5 is sufficient to convert the intermediate DME to hydrocarbons. To determine the effect of the mass ratio of CZA to SAPO-5 on the reactivity, additional experiments were conducted. The results displayed in Table 4 and Table S6 show that the yield of hydrocarbons and selectivity for C_3–C_5 hydrocarbons were highest when the bifunctional catalyst with the weight ratio of SAPO-5/CZA of about 4. When the mass ratio of SAPO-5 to CZA was 3 or less, a large amount of DME was observed in the products, which is undesirable for the production of hydrocarbons, although the total yield of the products was high. It means that the hybrid catalyst has insufficient active sites to convert DME to hydrocarbon. With the increase in the content of SAPO-5, the conversion of CO increased firstly, reached the maximum (at the ratio of SAPO-5 to CZA is 4) and then decreased quickly. When the mass ratio of SAPO-5 to CZA was more than 4, with the increase of CZA content in the bifunctional catalysts, the CO conversion increased, which may be ascribed to that the formation of methanol is the control reaction in the process under this condition. With the increase of SAPO-5 content in the bifunctional catalysts, the selectivity for C_3–C_5 hydrocarbons increased firstly and then decreased. Therefore, the most effective bifunctional catalyst for selective synthesis of light hydrocarbons from syngas is the one that contains 20 wt% CZA methanol catalyst and 80 wt% SAPO-5 zeolite.

Table 4 Effect of the mass ratio of SAPO-5 to CAZ in the bifunctional catalysts on catalytic performance of CZA/SAPO-5-0.4

SAPO-5/CZA	X_{CO} (%)	Hydrocarbon product distribution (%)			
		C_1	C_2	C_3–C_5	C_{6+}
2	22.8	5.2	16.6	73.0	5.2
3	23.4	3.9	10.2	81.4	4.4
4	24.0	4.4	5.6	86.1	3.9
5	20.5	7.1	7.5	82.8	2.6
6	16.9	11.8	6.0	81.6	0.7

Reaction conditions: $p = 4.0$ MPa, $GHSV = 9600$ h^{-1}, $n(H_2)/n(CO) = 2.3$, $T = 300$ °C, reaction time 1 h

DME dimethyl ether

3.2.4 Catalytic Performance of the CZA/SAPO-5 Bifunctional Catalysts: Effect of the Zeolite Acidity

Allow for the significance of the acidity of the methanol dehydration catalyst to the syngas to hydrocarbons reaction, catalysts composed of SAPO-5 with varied Si/Al ratio and fixed amount of methanol synthesis component (CZA) were introduced to investigate the effect of acidity on the performance of the bifunctional catalyst in detail, especially the acidic density and type. According to the main reactions involved in the syngas to hydrocarbons process, the acid catalyst could remove the methanol formed through Reaction (1), thus shifting the equilibrium of reaction to the right-hand side. Correspondingly, as shown in Table S7 and Fig. 4, the increase in the density of acid sites increased CO conversion over the CZA/SAPO-5 catalyst as expected. In order to identify the type of the zeolite acid sites involved in the methanol dehydration reaction under the studied conditions, several

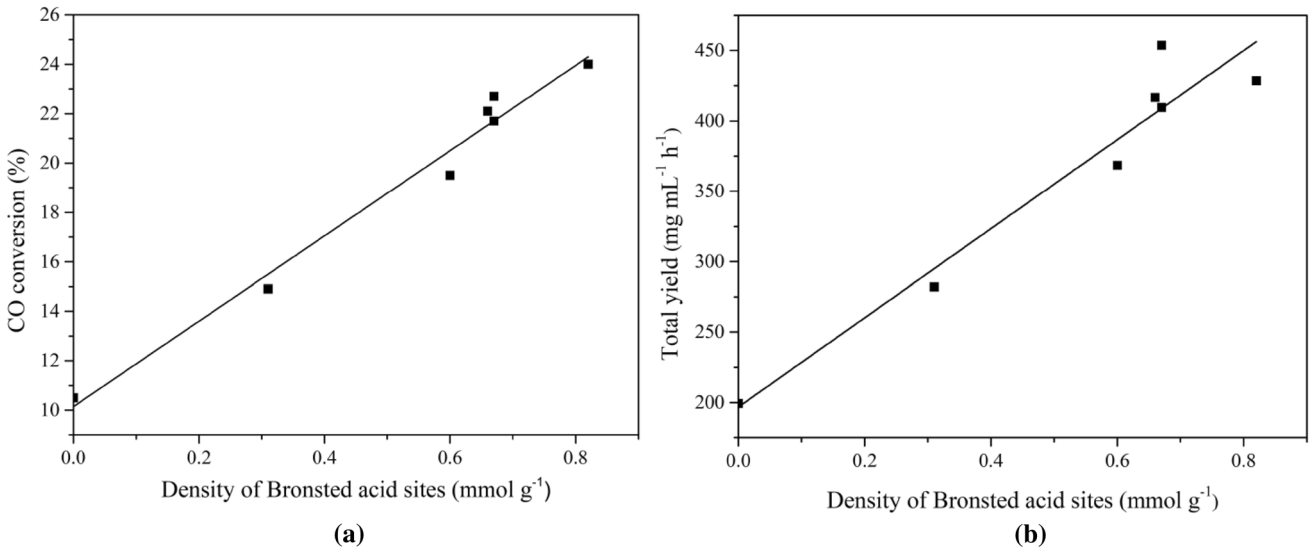

Fig. 4 Correlation between the CO conversion (**a**) or total yield (**b**) and the density of Brönsted acid sites during the syngas to hydrocarbon experiments on CZA/SAPO-5-x catalysts under the given conditions. Reaction conditions: mass ratio of CZA: SAPO-5 = 1:4; p = 4.0 MPa, $GHSV$ = 9600 h^{-1}, $n(H_2)/n(CO)$ = 2.3, reaction time 1 h

attempts were made to correlate the CO conversion and the total yield with the zeolite acid properties. Consequently, a fairly nice linear correlation between the CO conversion and the density of Brönsted acid sites was evidenced (Fig. 4a), suggesting that under the employed reaction conditions the overall syngas to hydrocarbons reaction was controlled by the methanol dehydration step and the dehydration activity of the acid component was mainly determined by the Brönsted acid sites. Besides, when AlPO-5 with few Brönsted acid sites was used instead of SAPO-5 in the bifunctional catalyst, only a small amount of hydrocarbons formed, making DME the main product. In contrast, complete conversion of DME could be achieved when SAPO-5-0.1 with relatively fewer Brönsted acid sites was employed. The above experimental results further confirm that the dehydration of DME to hydrocarbons takes place mainly on the Brönsted acid sites. Furthermore, the best linear correlation coefficient (R^2) was also obtained when the total yield is plotted against the density of Brönsted acid sites (Fig. 4b). These results indicated that the efficiency for the one-step synthesis of hydrocarbons from syngas of the CZA/SAPO-5 catalysts was directly proportional to the Brönsted acid sites density of the zeolite under dehydration-controlled conditions.

The hydrocarbon distributions over the catalyst with different acid sites density are presented in Fig. 5. It can be observed that the selectivity of C_2 increased and that of C_3–C_5 fractions decreased with an increase in the density of Brönsted acid sites to 0.67 mmol g^{-1}. However, a larger density of Brönsted acid sites (0.82 mmol g^{-1}) reduced the selectivity of C_2 and increased that of C_3–C_5 hydrocarbons. This is probably because the MTH reaction

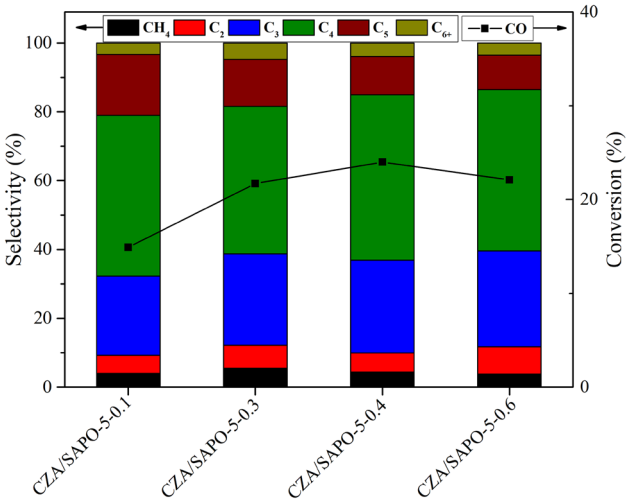

Fig. 5 Product selectivity and CO conversion over CZA/SAPO-5 catalysts with different Si/Al ratio for conversion of syngas to light hydrocarbons. Reaction conditions: mass ratio of CZA: SAPO-5 = 1:4, p = 4.0 MPa, $GHSV$ = 9600 h^{-1}, $n(H_2)/n(CO)$ = 2.4, T = 300 °C, reaction time 1 h

proceeds through a dual cycle mechanism on SAPO-5 and with increasing Brönsted acid site density, the aromatic-based cycle was much more favored than the olefin-based cycle, leading to a higher selectivity to C_2 fractions. However, further increasing the Brönsted acid site densities to 0.82 mmol g^{-1}, more light olefins were converted into hydrocarbons with high carbon number over acid sites by chain growth reactions. For SAPO-0.5 and SAPO-0.6 catalysts with similar Brönsted acid site density but higher

acid strength compared with SAPO-5-0.3, the secondary reaction of products such as over cracking of heavy hydrocarbons intensified, and thus caused extra light paraffins and less C_{6+} hydrocarbons. In short, over the CZA/zeolite bifunctional catalysts, syngas is converted into methanol on CZA and the methanol turns into light olefins over the active sites of zeolite. Most of light olefins would transfer to CZA and participate in a hydrogenation reaction to form light paraffins in the hydrogen atmosphere over the copper active sites of CZA. Meanwhile, some olefins would convert into heavy hydrocarbons through chain growth reactions over acid sites. Thus, the bifunctional catalyst should have an appropriate density and strength of Brönsted acid sites to achieve the best catalytic performance.

4 Conclusion

In this work, one-step transformation of syngas to light hydrocarbons was investigated over SAPO-5 physically mixed with a methanol synthesis catalyst CuO–ZnO–Al_2O_3. It was demonstrated that the zeolites employed in the bifunctional catalysts are critical to the activity and selectivity of the catalysts and the use of SAPO-5 zeolite was more promising for the direct production of light hydrocarbons (C_3–C_5) from syngas, differed from large-pore aluminosilicate zeolites. A time–space yield of 461.6 mg mL^{-1} h^{-1} and 88.1% selectivity to C_3–C_5 hydrocarbons could be attained from syngas over the CZA/SAPO-5-0.4 catalyst at 290 °C. The high activity of the bifunctional catalyst with SAPO-5 could be attributed to its appropriate topological structure and moderate acidity. Temperatures between 260 and 320 °C and the mass ratio of CZA to SAPO-5 between 1:1 and 1:6 were evaluated using a molar feed syngas ratio (H_2/CO) of 2.3. Operating at a relatively low temperature of 290 °C resulted in enhanced C_3–C_5 production and diminished undesirable C_1 and DME production. Lower temperature operation also resulted in enhanced CO conversion. Furthermore, through systematic studies using catalysts with varied Brönsted acidity, it was clarified that the dehydration of DME to hydrocarbons takes place mainly on the Brönsted acid sites. Under dehydration-controlled conditions, the efficiency for the one-step synthesis of hydrocarbons from syngas of the CZA/SAPO-5 catalysts is directly proportional to the Brönsted acid sites density of the zeolite. A moderate density and strength of Brönsted acid sites in the SAPO-5 zeolite would suppress the formation of methane and C_{6+} hydrocarbons and achieve the best catalytic performance.

Acknowledgements This work was supported by the China Postdoctoral Science Foundation (2018M642769) for the financial supports.

References

1. Yang S, Xiao L, Yang S, Kraslawski A, Man Y, Qian Y (2014) ACS Sustain Chem Eng 2:80. https://doi.org/10.1021/sc400336e
2. Zhang S, Li D, Liu Y, Zhang Y, Wu Q (2019) Catal Lett 149:1486. https://doi.org/10.1007/s10562-019-02775-x
3. Cheng K, Zhang L, Kang J, Peng X, Zhang Q, Wang Y (2015) Chem Eur J 21:1928. https://doi.org/10.1002/chem.201405277
4. Yang J, Gong K, Miao D, Jiao F, Pan X, Meng X, Xiao F, Bao X (2019) J Energy Chem 35:44. https://doi.org/10.1016/j.jechem.2018.10.008
5. Kondratenko EV, Peppel T, Seeburg D, Kondratenko VA, Kalevaru N, Martin A, Wohlrab S (2017) Catal Sci Technol 7:366. https://doi.org/10.1039/C6CY01879C
6. Batamack PTD, Mathew T, Prakash GKS (2017) J Am Chem Soc 139:18078. https://doi.org/10.1021/jacs.7b10725
7. Alayat A, Mcllroy DN, McDonald AG (2018) Fuel Process Technol 169:132. https://doi.org/10.1016/j.fuproc.2017.09.011
8. Nie C, Zhan H, Ma H, Qian W, Sun Q, Ying W (2019) Catal Lett 149:1375. https://doi.org/10.1007/s10562-019-02700-2
9. Xue Y, Ge H, Chen Z, Zhai Y, Zhang J, Sun J, Abbas M, Lin K, Zhao W, Chen J (2018) J Catal 358:237. https://doi.org/10.1016/j.jcat.2017.12.017
10. Xu K, Sun B, Lin J, Wen W, Pei Y, Yan S, Qiao M, Zhang X, Zong B (2014) Nat Commun 5:5783. https://doi.org/10.1038/ncomms6783
11. Hibbitts D, Dybeck E, Lawlor T, Neurock M, Iglesia E (2016) J Catal 337:91. https://doi.org/10.1016/j.jcat.2016.01.010
12. Dry ME (2002) Catal Today 71:227. https://doi.org/10.1016/S0920-5861(01)00453-9
13. Wang C, Yang J, Sun Y, Li Q, Zheng Y, Hu YH (2019) Fuel 244:395. https://doi.org/10.1016/j.fuel.2019.02.024
14. Zhao B, Zhai P, Wang P, Li J, Li T, Peng M, Zhao M, Hu G, Yang Y, Li YW, Zhang Q, Fan W, Ma D (2017) Chem 3:323. https://doi.org/10.1016/j.chempr.2017.06.017
15. Harmel J, Peres L, Estrader M, Berliet A, Maury S, Fécant A, Chaudret B, Serp P, Soulantica K (2018) Angew Chem Int Ed 57:10579. https://doi.org/10.1002/anie.201804932
16. Li J, Pan X, Bao X (2015) Chin J Catal 36:1131. https://doi.org/10.1016/S1872-2067(14)60297-7
17. Chinchen GC, Denny PJ, Parker DG, Spencer MS, Whan DA (1987) Appl Catal 30:333. https://doi.org/10.1016/S0166-9834(00)84123-8
18. Deng X, Liu Y, Huang W (2018) J Energy Chem 27:319. https://doi.org/10.1016/j.jechem.2017.10.007
19. Kim J-H, Park MJ, Kim SJ, Joo O-S, Jung K-D (2004) Appl Catal A 264:37. https://doi.org/10.1016/j.apcata.2003.12.058
20. Kuld S, Thorhauge M, Falsig H, Elkjær CF, Helveg S, Chorkendorff I, Sehested J (2016) Science 352:969. https://doi.org/10.1126/science.aaf0718
21. Behrens M, Studt F, Kasatkin I, Kühl S, Hävecker M, Abild-Pedersen F, Zander S, Girgsdies F, Kurr P, Kniep B-L, Tovar M, Fischer RW, Nørskov JK, Schlögl R (2012) Science 336:893. https://doi.org/10.1126/science.1219831
22. Chen Y, Xu Y, Cheng D-G, Chen Y, Chen F, Lu X, Huang Y, Ni S (2015) J Chem Technol Biotechnol 90:415. https://doi.org/10.1002/jctb.4309
23. Nieskens DLS, Ciftci A, Groenendijk PE, Wielemaker MF, Malek A (2017) Ind Eng Chem Res 56:2722. https://doi.org/10.1021/acs.iecr.6b04643
24. Zhang Q, Li X, Asami K, Asaoka S, Fujimoto K (2005) Catal Lett 102:51. https://doi.org/10.1007/s10562-005-5202-x
25. Ge Q, Lian Y, Yuan X, Li X, Fujimoto K (2008) Catal Commun 9:256. https://doi.org/10.1016/j.catcom.2007.06.011

26. Lu P, Shen D, Cheng S, Hondo E, Chizema LG, Wang C, Gai X, Lu C, Yang R (2018) Fuel 223:157. https://doi.org/10.1016/j.fuel.2018.02.159
27. Ma X, Ge Q, Ma J, Xu H (2013) Fuel Process Technol 109:1. https://doi.org/10.1016/j.fuproc.2013.01.002
28. Zhang Q, Li X, Asami K, Asaoka S, Fujimoto K (2004) Fuel Process Technol 85:1139. https://doi.org/10.1016/j.fuproc.2003.10.016
29. Li C, Yuan X, Fujimoto K (2014) Appl Catal A 475:155. https://doi.org/10.1016/j.apcata.2014.01.025
30. Ereña J, Arandes JM, Bilbao J, Olazar M, de Lasa HI (1999) J Chem Technol Biotechnol 72:190. https://doi.org/10.1002/(SICI)1097-4660(199806)72:2%3c190:AID-JCTB895%3e3.0.CO;2-8
31. Mysov VM, Reshetnikov SI, Stepanov VG, Ione KG (2005) Chem Eng J 107:63. https://doi.org/10.1016/j.cej.2004.12.011
32. Dagle RA, Lizarazo-Adarme JA, Lebarbier Dagle V, Gray MJ, White JF, King DL, Palo DR (2014) Fuel Process Technol 123:65. https://doi.org/10.1016/j.fuproc.2014.01.041
33. Lorenz E, Wehling P, Schlereth M, Kraushaar-Czarnetzki B (2016) Catal Today 275:183. https://doi.org/10.1016/j.cattod.2016.03.004
34. Flores JH, da Silva MIP (2016) Catal Lett 146:1505. https://doi.org/10.1007/s10562-016-1771-0
35. Haw JF, Song W, Marcus DM, Nicholas JB (2003) Acc Chem Res 36:317. https://doi.org/10.1021/ar020006o
36. Wang C, Ma X, Ge Q, Xu H (2015) Catal Sci Technol 5:1847. https://doi.org/10.1039/C4CY01494D
37. Cheng K, Zhou W, Kang J, He S, Shi S, Zhang Q, Pan Y, Wen W, Wang Y (2017) Chem 3:334. https://doi.org/10.1016/j.chempr.2017.05.007
38. Gayubo AG, Benito PL, Aguayo AT, Olazar M, Bilbao J (1996) J Chem Technol Biotechnol 65:186. https://doi.org/10.1002/(SICI)1097-4660(199602)65:2%3c186:AID-JCTB401%3e3.0.CO;2-J
39. Wang L, Guo C, Yan S, Huang X, Li Q (2003) Micropor Mesopor Mater 64:63. https://doi.org/10.1016/S1387-1811(03)00482-7
40. Guisnet M, Ayrault P, Datka J (1997) Pol J Chem 71:1455
41. van Bennekom JG, Venderbosch RH, Winkelman JGM, Wilbers E, Assink D, Lemmens KPJ, Heeres HJ (2013) Chem Eng Sci 87:204. https://doi.org/10.1016/j.ces.2012.10.013
42. García-Trenco A, Martínez A (2012) Appl Catal A 411–412:170. https://doi.org/10.1016/j.apcata.2011.10.036
43. Yuen L-T, Zones SI, Harris TV, Gallegos EJ (1994) Micropor Mater 2:105. https://doi.org/10.1016/0927-6513(93)E0039-J
44. Westgård Erichsen M, Svelle S, Olsbye U (2013) J Catal 298:94. https://doi.org/10.1016/j.jcat.2012.11.004
45. Westgård Erichsen M, Svelle S, Olsbye U (2013) Catal Today 215:216. https://doi.org/10.1016/j.cattod.2013.03.017
46. Lebarbier VM, Dagle RA, Kovarik L, Lizarazo-Adarme JA, King DL, Palo DR (2012) Catal Sci Technol 2:2116. https://doi.org/10.1039/C2CY20315D

Publisher's Note Springer Nature remains neutral with regard to jurisdictional claims in published maps and institutional affiliations.

Affiliations

Tao Liu[1] · Tianliang Lu[2] · Mingming Yang[1] · Lipeng Zhou[1] · Xiaomei Yang[1] · Beibei Gao[1] · Yunlai Su[1]

[1] College of Chemistry and Molecular Engineering, Zhengzhou University, 100 Kexue Road, Zhengzhou 450001, People's Republic of China

[2] School of Chemical Engineering and Energy, Zhengzhou University, 100 Kexue Road, Zhengzhou 450001, People's Republic of China